

Exploring dust formation in the episodic WCd system WR140

J. W. Eatson[★], J. M. Pittard & S. Van Loo

School of Physics and Astronomy, University of Leeds, Woodhouse Lane, Leeds LS2 9JT, UK

Accepted XXX. Received YYY; in original form ZZZ

ABSTRACT

Key words: stars: Wolf-Rayet – methods: numerical – binaries: general

1 INTRODUCTION

In this paper we will discuss our methodology in section

2 METHODOLOGY

The periodic dust forming system WR140 was simulated using a fork of the Athena++ hydrodynamical code (Stone et al. 2020), a series of modifications were implemented to simulate binary system orbits, stellar wind outflows and dust evolution. These simulations were conducted in 3D in a Cartesian co-ordinate system. The code solves a Riemann problem at each cell interface to determine the time-averaged values at the zone interfaces, and then solves the equations of hydrodynamics:

$$\frac{\partial \rho}{\partial t} + \nabla \cdot (\rho \mathbf{u}) = 0, \quad (1a)$$

$$\frac{\partial \rho \mathbf{u}}{\partial t} + \nabla \cdot (\rho \mathbf{u} \mathbf{u} + P) = 0, \quad (1b)$$

$$\frac{\partial \rho \varepsilon}{\partial t} + \nabla \cdot [\mathbf{u} (\rho \varepsilon + P)] = \dot{E}_{\text{cool}}, \quad (1c)$$

where ε is the total specific energy ($\varepsilon = \mathbf{u}^2/2 + e/\rho$), ρ is the mass density, e is the internal energy density, P is the gas pressure and \mathbf{u} is the gas velocity. In order to simulate radiative losses, the parameter \dot{E}_{cool} is included, which is the energy loss rate per unit volume from the fluid due to gas and dust cooling.

Spatial reconstruction using a piecewise linear method was performed, while the time-integration scheme is a third-order accurate, three-stage strong stability preserving Runge-Kutta¹ method (Gottlieb et al. 2009). Several passive scalars are utilised to model wind mixing and dust evolution, the scalar values are transported by the fluid, for a given scalar species i , the scalar is advected through the scalar through the following equation:

$$\rho \frac{dC_i}{dt} = \frac{\partial}{\partial t} (\rho C_i) + \nabla \cdot (C_i \rho \mathbf{u}) = -\nabla \cdot \mathbf{Q}_i, \quad (2)$$

where $\mathbf{Q}_i = -\nu_{ps} \rho \nabla C_i$ is the diffusive flux density and ν is the passive scalar diffusion coefficient (Stone et al. 2020).

Stellar winds are simulated by modifying the density, ρ_R , momentum, p_R , and energy, E_R in a small region around both stars. Winds flow from this “remap” region at the stars wind terminal velocity, v^∞ . Remap zone parameters are calculated with the formulae

$$\rho_R = \frac{\dot{M}}{4\pi r^2 v_\infty}, \quad (3a)$$

$$p_R = \rho_R v_r, \quad (3b)$$

$$E_R = \frac{P_R}{\gamma - 1} + \frac{1}{2} \rho_R v_\infty^2, \quad (3c)$$

where P_R is the cell pressure, $P_R = \rho_R k_B T_w / \mu m_H$, T_w is the wind temperature, μ is the mean molecular mass, m_H is the mass of a hydrogen atom, v_R is the wind velocity as it flows radially from the center of the “remap zone” and r is the distance from the current cell to the centre of the remap zone. This method produces radially out-flowing winds from the star with an expected density and velocity. This method is stable against numerical instability, while also allowing us to precisely control the winds.

Line driving and wind acceleration effects are not simulated, which can result in divergence with the correct wind velocity as stars approach periastron passage. Instead, winds are instantaneously accelerated to their terminal velocity. Additionally, influence from either gravitational self-interaction and interaction with the stars gravity wells is not simulated, with the stellar winds assumed to be travelling far in excess of the system escape velocity.

Adaptive Mesh Refinement was considered for this simulation, however a known issue with the Athena++ code prevented this from being possible. Passive scalars incorporated into the simulation were found to not be conserved along the interfaces between mesh blocks undergoing refinement, this meant that the simulation would behave non-physically (This bug is recorded as issue #365 on the Athena++ Github repository²). A ring of refined cells across the orbital path was considered, but the performance improvements of this method were found to be negligible and not worth pursuing, as the block based refinement method of Athena++ would result in much redundant refinement. Instead, a static mesh is used, where a region around the

[★] E-mail: py13je@leeds.ac.uk

¹ SSPRK (3,3)

² <https://github.com/PrincetonUniversity/athena/issues/365>

stars at $\phi = 0.95$ is refined to the maximum level, with a gradual de-refinement away from this refinement region.

2.1 Dust model and cooling

The dust model in this paper simulates dust growth and destruction through collisions between carbon atoms and dust grains. These grains are simulated in the form of advected scalars in each cell in the numerical grid which propagate with the same hydrodynamical rules as the stellar wind; as such dust can be described as co-moving with the interstellar wind. The two scalars in use are z , the dust-to-gas mass ratio within the cell, and a , the average grain radius. Using these parameters in addition to the local wind parameters, the dust can be adequately described and evolved with time.

A number of assumptions are made in this dust model, for instance, the dust grains are assumed to be spherical, with a uniform density of 3.0 g cm^{-3} . Dust grains are assumed to have a single size in a region, as well as a constant number density, as such, this model does not simulate grain agglomeration and fracturing. Additional mechanisms for dust formation and destruction could also be implemented such as grain-grain agglomeration and photoevaporation. Furthermore, a multi-fluid model with drag force coupling could also be implemented, however this is beyond the scope of this paper.

Dust is grown through grain accretion using formulae described by (Spitzer 2008). Dust grains grow via collisions with the surrounding gas, as gas accretes onto these grains the associated density is subtracted from the gas density. The growth rate is such that:

$$\frac{da}{dt} = \frac{\xi_a \rho_{Gr} w_a}{4\rho}, \quad (4a)$$

$$\frac{\rho_D}{dt} = 4\pi a^2 \rho n_D \frac{da}{dt}, \quad (4b)$$

where w_a is the Maxwell-Boltzmann distribution RMS velocity, ξ_a is the grain sticking efficiency, ρ_{Gr} is the grain bulk density, ρ is the gas density, a is the dust grain radius, and n_D is the grain number density. For these simulations, the grain sticking factor has been set to 10%, while for low temperature collisions a sticking factor of 100% can be proven, grain sticking in a more energetic, hot regime could significantly reduce the probability of sticking.

Dust destruction is calculated via gas-grain sputtering using the Draine & Salpeter prescription - a dust grain has a lifespan, τ , which is dependent on the grain radius, as the grain loses radius proportional to its loss in mass; assuming a spherical grain, the rate of change in mass and radius can be calculated through the following equation:

$$\tau_D = 1 \text{ Myr} \times \frac{a}{n_g}, \quad (5a)$$

$$\frac{da}{dt} = -\frac{a}{\tau_D}, \quad (5b)$$

$$\frac{dm}{dt} = -1.33 \times 10^{-13} a^2 n_g n_D \rho_{Gr}, \quad (5c)$$

3 WR140 AND SIMULATION PARAMETERS

WR 140 was simulated for this paper as it represents an archetypical episodic CWB system, whose infrared dust emission peaks around periastron passage. WR 140 deviates from WR 98a and WR 104 by being extremely eccentric, which significantly effects the cooling parameter as the orbit progresses. Additionally, the minimum value

| | | |
|-------------------|--|------------------------|
| M_{WR} | $10.31 M_{\odot}$ | Thomas et al. (2021) |
| M_{OB} | $29.27 M_{\odot}$ | Thomas et al. (2021) |
| P | 7.926 yr | Thomas et al. (2021) |
| e | 0.8993 | Thomas et al. (2021) |
| \dot{M}_{WR} | $5.6 \times 10^{-5} M_{\odot} \text{ yr}^{-1}$ | Williams et al. (1990) |
| \dot{M}_{WR} | $1.6 \times 10^{-6} M_{\odot} \text{ yr}^{-1}$ | Williams et al. (1990) |
| v_{WR}^{∞} | $2.86 \times 10^3 \text{ km s}^{-1}$ | Williams et al. (1990) |
| v_{OB}^{∞} | $3.20 \times 10^3 \text{ km s}^{-1}$ | Williams et al. (1990) |
| η | 0.031 | Calculated |
| χ_{min} | 2.69 | Calculated |

Table 1. WR140 system parameters.

| | X(E) | |
|----|-------|-------|
| | Solar | WC |
| H | 0.705 | 0.000 |
| He | 0.275 | 0.546 |
| C | 0.003 | 0.400 |
| N | 0.001 | 0.000 |
| O | 0.010 | 0.050 |

Table 2. Abundances used for the OB and WR stars being simulated. Other elements are assumed trace when calculating dust emission (Williams et al. 2015).

for χ is significantly larger than the other systems, and hence cooling would be less dominant on the dynamics of the WCR, even at periastron. Though these simulations do not calculate wind acceleration due to radiative line driving, both stellar winds are expected to be accelerated close to their terminal wind velocities (Lamers & Cassinelli 1999). However, this discrepancy should be noted when considering the results of this paper. Recent improved estimations of the orbital parameters of WR140 by Thomas et al. (2021) were used to calculate the orbital path for these simulations (see Table 1). In order to correctly calculate cooling and dust growth, the abundances of hydrogen, helium, and metals, particularly CNO must be included in the simulations parameters. A typical wind composition for WC stars was assumed for the Wolf-Rayet star, while a solar abundance was assumed for the OB star (Table 2).

Due to computing limitations, a complete orbit could not be completed without AMR, instead, a section of the systems orbit, corresponding to an orbital phase of $0.95 \leq \Phi \leq 1.10$ was simulated, where Φ is the orbital phase. This section represents the period prior to periastron passage, as well as a brief period after periastron (fig. 1). This represents a period of approximately 1.2 years of the systems orbit, and the period where much of the dust forms (Crowther 2003). The simulation was run with two different numerical integrators, a 3rd order accurate Runge-Kutta integrator (rk3) and a 4th order accurate, 5-stage, 3 storage register strong stability preserving Runge-Kutta integrator (ssprk5_4) (Ruuth & Spiteri 2005). The ssprk5_4 integrator was found to be approximately 60% slower, but markedly more stable. Prior to periastron passage the rk3 integrator was used for its speed, but increasing numerical instability as the stars grew closer resulted in this proving untenable. Over periastron passage the average time-step was found to reduce by an order of magnitude, resulting in a corresponding increase to simulation time (fig. 2). At the most numerically complex portion of the work, a Courant number of $C = 0.04$ has to be used instead of the initial value of $C = 0.15$. This reduced value was used to preserve numerical stability.

The simulation was conducted on the ARC4 HPC cluster at the University of Leeds with 128 cores. The code was compiled using

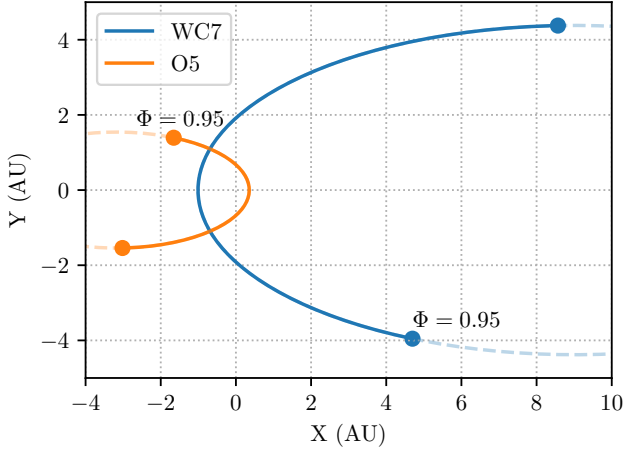


Figure 1. Simulation orbital trajectories of the WC7 and O5 stars in WR140. The solid line represents the orbital phase being simulated, corresponding to $0.95 \leq \Phi \leq 1.10$. The simulation starting position for each star has been annotated.

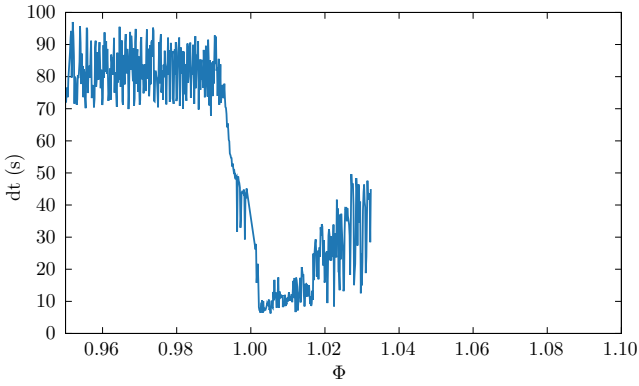


Figure 2. Timestep, dt , over the course of the WR140 simulation. after periastron passage the `ssprk5_4` numerical integrator and a drastically reduced Courant number was adopted in order to preserve numerical stability. This increased simulation time by approximately an order of magnitude.

the Intel ICPC compiler using AVX512 optimisations and the Intel MPI library.

REFERENCES

- Crowther P. A., 2003, *Astrophysics and Space Science*, 285, 677
 Gottlieb S., Ketcheson D. I., Shu C.-W., 2009, *J Sci Comput*, 38, 251
 Lamers H. J., Cassinelli J. P., 1999, *Introduction to Stellar Winds*. Cambridge University Press
 Ruuth S. J., Spiteri R. J., 2005, *SIAM Journal on Numerical Analysis*, 42, 974
 Spitzer L., 2008, *Physical Processes in the Interstellar Medium*. John Wiley & Sons
 Stone J. M., Tomida K., White C. J., Felker K. G., 2020, *ApJS*, 249, 4
 Thomas J. D., et al., 2021, *Monthly Notices of the Royal Astronomical Society*, 504, 5221
 Williams P. M., van der Hucht K. A., Pollock A. M. T., 1990, *Monthly Notices of the Royal Astronomical Society*, 243, 662

Williams P. M., Crowther P. A., van der Hucht K. A., 2015, *Monthly Notices of the Royal Astronomical Society*, 449, 1834

This paper has been typeset from a \LaTeX file prepared by the author.